

Fast and Robust Localization for Humanoid Soccer Robot via Iterative Landmark Matching

Ruo Chen Hou¹, Mingzhang Zhu¹, Hyunwoo Nam¹, Gabriel I. Fernandez¹, and Dennis W. Hong¹

Abstract—Accurate robot localization is essential for effective operation. Monte Carlo Localization (MCL) is commonly used with known maps but is computationally expensive due to landmark matching for each particle. Humanoid robots face additional challenges, including sensor noise from locomotion vibrations and a limited field of view (FOV) due to camera placement. This paper proposes a fast and robust localization method via iterative landmark matching (ILM) for humanoid robots. The iterative matching process improves the accuracy of the landmark association so that it does not need MCL to match landmarks to particles. Pose estimation with the outlier removal process enhances its robustness to measurement noise and faulty detections. Furthermore, an additional filter can be utilized to fuse inertial data from the inertial measurement unit (IMU) and pose data from localization. We compared ILM with Iterative Closest Point (ICP), which shows that ILM method is more robust towards the error in the initial guess and easier to get a correct matching. We also compared ILM with the Augmented Monte Carlo Localization (aMCL), which shows that ILM method is much faster than aMCL and even more accurate. The proposed method’s effectiveness is thoroughly evaluated through experiments and validated on the humanoid robot ARTEMIS during RoboCup 2024 adult-sized soccer competition.

I. INTRODUCTION

RoboCup is an international robot soccer competition where accurate localization is crucial for decision-making and path planning [1]. Real-time localization with limited computational resources requires fast and efficient algorithms, as delays in localization affect path planning and trajectory tracking performance. Therefore, fast and accurate localization is essential for our humanoid platform, ARTEMIS, which can move at speeds up to 1.5 m/s. Since ARTEMIS walks on a 2D plane, the localization problem is inherently simplified to 2D in this paper.

Unlike wheel-based robots, bipedal locomotion and motor vibrations introduce more noise to the sensors. Additionally, to closely mimic human movement, the competition restricts the use of sensors to only the camera mounted on the actuated neck, further complicating the localization challenge. Traditional visual odometry (VO) based methods [2], which rely on tracking visual features between consecutive frames, are not suitable due to the presence of moving people and robots on the field, which can significantly affect VO accuracy. Kinematic-based methods are also prone to inaccuracies, especially due to sliding on the grass. Learning based methods [3], while effective, require training on specific

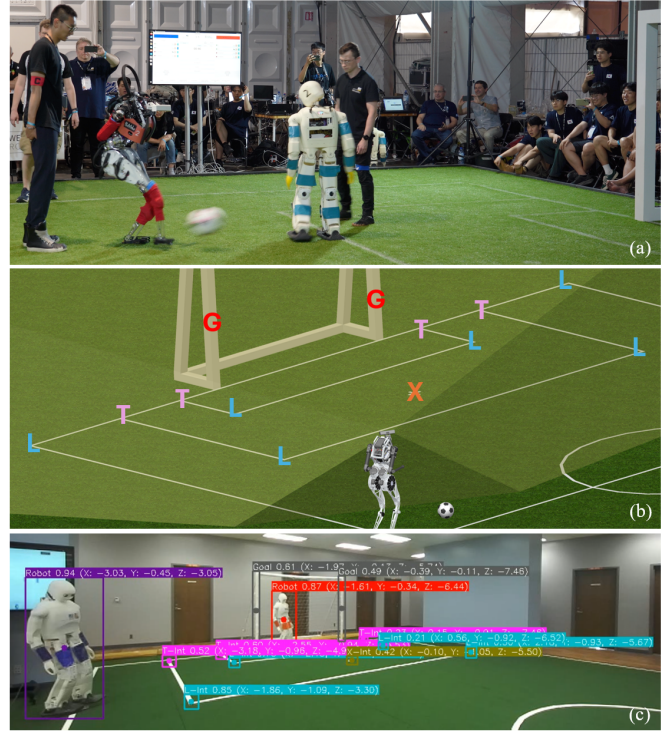


Fig. 1: (a) Picture from RoboCup 2024’s championship match [4] with our robot, ARTEMIS, shown in red taking a shot on goal from far away. A person dressed in black carries an emergency stop behind ARTEMIS for safety. (b) A 3D simulated environment where the yellow polyhedron represents the camera’s field of view in 3D. The mapped field features, including goal posts marked with a red *G*, corners denoted with a green *L*, t-intersections with a pink *T*, and crosses with a yellow *X*. (c) Illustrates landmarks, goal post and robots detection using the ZED 2i camera.

images from a given location, making them impractical and time-consuming for tournament settings.

Given that the details of the soccer field are provided ahead of time, we can use the field features as input to estimate the robot’s pose. Approaches utilizing field lines have been explored [5]–[9], as well as methods using pre-defined landmarks such as corners, T-intersections, crosses, and goalposts [10], [11], as shown in Fig. 1. Matching pre-defined landmarks is easier than using lines, as the robot can detect multiple landmarks but typically cannot see the entire line. Furthermore, YOLO-based landmark detection [10], [11] is fast and accurate. In this work, we used a YOLOv8 network trained on a custom landmark data set to identify these landmarks.

A common method for localization on a known map like a soccer field is Monte-Carlo localization (MCL) using the landmarks on the field [7], [10], [12]–[15]. The MCL method uses particles to explore the possible states, evaluate them,

¹Robotics and Mechanisms Laboratory (RoMeLa), Department of Mechanical and Aerospace Engineering, University of California, Los Angeles, CA 90095, USA. {houruo chen, normanzmz, harrynam, gabriel1808, dennishong}@ucla.edu

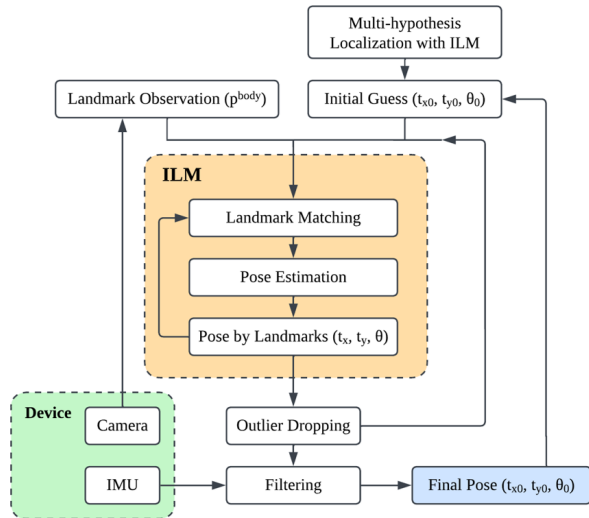


Fig. 2: Work flow of our localization method. ILM takes the landmark observation and initial guess for its pose as an input. It then matches and estimates the pose iteratively and drops outliers. The pose from ILM is fused with data from an inertial measurement unit (IMU) using a filter to get the final localized state.

and assign weights to those particles. However, the MCL method needs to match and evaluate landmarks for each particle, which is computationally heavy and slow, especially for a large number of particles.

To address this issue, we propose iterative landmark matching (ILM) to improve the matching accuracy. Our method directly calculates the pose from the matched landmarks, eliminating the need for MCL to explore multiple particles. Fig. 2 shows the proposed localization framework. Initially, Multi-Hypothesis Localization (MHL) is used to localize the starting pose. ILM takes the landmark observation and the previous pose as an initial guess, iteratively matches and estimates the pose, and removes outliers. The estimated pose is then fused with IMU data through a filter to obtain the localized state of the robot.

This article is organized as follows: In Section II, we discuss the existing methods related to our method. In Section III, we present our localization framework. The experimental results are presented and discussed in Section IV, where we compare ILM with ICP and aMCL, demonstrating its strong performance. All computations were performed on a Dell G16 laptop with an Intel Core i7-13650HX processor. Simulations used a 110-degree field of view (FOV), matching the ZED 2i camera used in the competition.

II. RELATED WORK

A. Iterative Closest Point

The Iterative Closest Point (ICP) algorithm, which was introduced by Besl and McKay [16], is a widely used method for point cloud registration. It iteratively refines the transformation by establishing correspondences based on the closest points and minimizing the alignment error. The classical point-to-point ICP uses nearest neighbor matching. There are also other variations, such as point-to-plane ICP [17], which improves accuracy by incorporating surface normals;

Generalized ICP (GICP) [18], which improves registration by using covariance-based metrics; and Deep Closest Point (DCP) [19] and PointNetLK [20], which are deep learning-based alternatives.

The ILM method can be considered a modification of ICP. One key difference is that ILM finds one-to-one matching, whereas ICP can result in multiple source points being matched to the same target point. One intuitive reason why ILM performs better than ICP in our case is that the landmarks are identified by YOLOv8. By design, YOLO [21] (including YOLOv8 [22]) does not assign two bounding boxes to the same object. Non-Maximum Suppression (NMS) is applied to remove redundant overlapping boxes, keeping only the one with the highest confidence score. Therefore, using the nearest point strategy to establish correspondences could incorrectly assign multiple landmarks to the same point on the map, which is typically inaccurate. This makes ICP more prone to getting trapped in local minima.

B. Data Association

Our approach begins by matching the landmarks observed by the stereo vision system to their corresponding landmarks in the known a priori map of the soccer field. The vision system detects landmarks such as corners, T-intersections, crosses, and goal posts relative to the robot. Matching these landmarks to their positions in the map can be formulated as a typical Linear Assignment Problem (LAP), defined as follows:

- A cost matrix $C \in \mathbb{R}^{n \times n}$, where C_{ij} represents the distance of assigning observed landmark i to target landmark j in the map. If C is not square, it can be made square by adding zero entries.
- A binary assignment matrix $Y \in \{0, 1\}^{n \times n}$, where $Y_{ij} = 1$ if observation i is assigned to target j , and $Y_{ij} = 0$ otherwise.

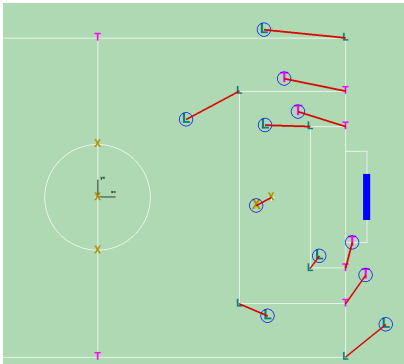
The goal is to minimize the total assignment cost:

$$\min_Y \sum_{i=1}^n \sum_{j=1}^n C_{ij} Y_{ij}$$

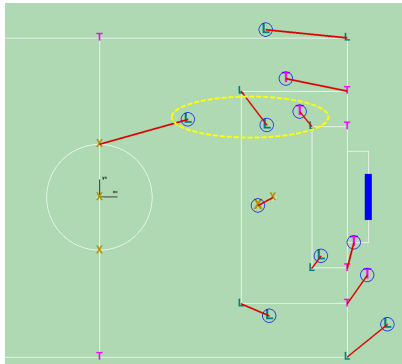
Subject to:

$$\sum_{j=1}^n Y_{ij} = 1, \sum_{i=1}^n Y_{ij} = 1, Y_{ij} \in \{0, 1\}, \forall i, j \in \{1, \dots, n\}$$

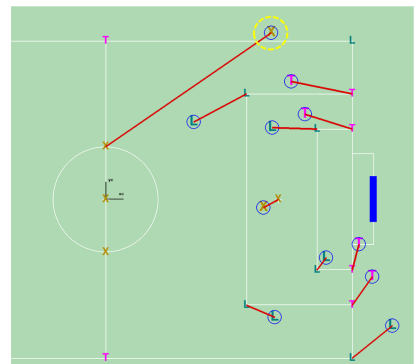
Different types of landmarks can be matched separately by creating distinct mappings based on their classification, or they can be treated identically by using the same mapping while ignoring their classification, as shown in Fig. 3. Matching landmarks of different types separately generally improves accuracy when the classification is correct. However, if some landmarks are misclassified—commonly occurring with landmarks that are far away or in poor lighting conditions—the matching accuracy may decrease. Therefore, we match the different types of landmarks both separately and identically in parallel, and then choose the result with the least error.



(a) Matching landmarks separately with no misclassification.



(b) Matching landmarks identically with no misclassification.



(c) Matching landmarks separately with misclassification.

Fig. 3: Landmark matching under different scenarios. This mismatched landmarks are circled in yellow. (a) shows the correct matching. (b) shows the mismatching due to treating different kinds of landmarks identically (c) shows the mismatching due to misclassification

The common methods for solving LAP are Kuhn–Munkres algorithm (Hungarian algorithm) [23], [24], Jonker-Volgenant algorithm [25], and integer linear programming [26]. We also note multiple improvements and modifications of the Jonker-Volgenant algorithm [27], [28]. The performance of methods is also compared in these papers [26], [29].

In our case, the number of points is relatively small, so what matters is guaranteeing the optimal solution in a fast enough time for real-time localization applications. Therefore, Kuhn–Munkres algorithm [24], Jonker-Volgenant algorithm [25] and the modified Jonker-Volgenant algorithm [28] are good candidates to use to solve LAP for our localization method.

We simulated the soccer field and timed the three methods by randomly sampling 100,000 poses uniformly across the field. The results show that the modified Jonker-Volgenant algorithm [28] is the fastest, taking 0.0537 ms in average. Therefore, we chose this method to match our landmarks.

C. Pose Estimation

The next component of our localization is to estimate the 2D pose according to the matched landmarks from Section II-B. The 2D pose of a robot includes the position transformation (t_x, t_y) and the orientation θ .

The problem is formulated as following. Given a set of points in the body frame p_i^{body} and the corresponding points in the world frame p_i^{world} , we need to find the 2D transformation (t_x, t_y, θ) which maps the body frame points to the world frame points. We define the translation vector as $t = (t_x, t_y)$, and the rotation angle as θ . The transformation can be expressed as:

$$p_i^{\text{world}} = R(\theta) \cdot p_i^{\text{body}} + t$$

where $R(\theta)$ is a 2D rotation matrix:

$$R(\theta) = \begin{bmatrix} \cos(\theta) & -\sin(\theta) \\ \sin(\theta) & \cos(\theta) \end{bmatrix}$$

Several methods that solve this include nonlinear programming (NLP), Direct Linear Transformation (DLT), and

the Kabsch algorithm [30]–[32]. The NLP method is flexible, handling various types of transformations and constraints. However, the methods for NLP, such as Sequential Quadratic Programming, Interior-Point Method, and Levenberg-Marquardt method, are computationally expensive. Moreover, NLP might give a local optimal solution which can be detrimental for our use case. The DLT method and Kabsch algorithm provide closed-form solutions [30]–[32] for the 2D pose, which are faster and better meet our needs.

III. LOCALIZATION FRAMEWORK

A. Iterative Landmark Matching

To correctly localize the robot, we need to match the landmarks detected correctly. The mismatching is a problem only if the initial guess of the 2D pose is far from the ground truth. One common method to deal with mismatching is MCL, which explores and evaluates particles in different poses, but it is computationally heavy. Our method for dealing with potential incorrect assignments is to iteratively correct the matching and remove potential outliers.

The algorithm is outlined in Algorithm 1. Given the initial guess for a pose $(t_{x_0}, t_{y_0}, \theta_0)$ and the landmark observation in the body frame p^{body} , calculate the corresponding position in world frame with an initial guess $p_{\text{guess}}^{\text{world}}$. Match the $p_{\text{guess}}^{\text{world}}$ to the map and find the landmark position in world frame p^{world} . Estimate the new pose $t_{x_i}, t_{y_i}, \theta_i$ as described in Section II-C. Repeat the landmark matching and pose estimation process until it reaches a predetermined maximum iteration limit or until the new pose converges.

We calculate the average calculation time for ILM with a maximum allowable iterations of 4. The average solving time for ILM using DLT is 0.901 ms and using Kabsh algorithm is 1.132 ms. Without considering the vision system, the ILM can be solved at approximately 1 kHz.

B. Global Localization

The soccer field is symmetric and the robot is not allowed to use magnetometers to find the direction. Therefore, robot will receive the same information in the symmetric pose.

Algorithm 1 Iterative Landmark Matching

```

1: Input:  $p^{\text{body}}, (t_{x_0}, t_{y_0}, \theta_0)$ 
2: Output:  $(t_{x_f}, t_{y_f}, \theta_f)$ 
3: Initialize  $p_{\text{guess}}^{\text{world}} = R(\theta_0)p^{\text{body}} + t_0$ , counter = 1
4: while counter < max_iteration do
5:    $p^{\text{world}} = \text{landmark\_matching}(p_{\text{guess}}^{\text{world}})$  (Section II-B)
6:    $t_{x_i}, t_{y_i}, \theta_i = \text{pose\_estimation}(p^{\text{world}}, p^{\text{body}})$  (Section II-C)
7:   if  $(t_{x_i}, t_{y_i}, \theta_i) = (t_{x_{i-1}}, t_{y_{i-1}}, \theta_{i-1})$  then
8:     break
9:   end if
10:  counter = counter + 1
11: end while
12: Return:  $(t_{x_f}, t_{y_f}, \theta_f)$ 

```

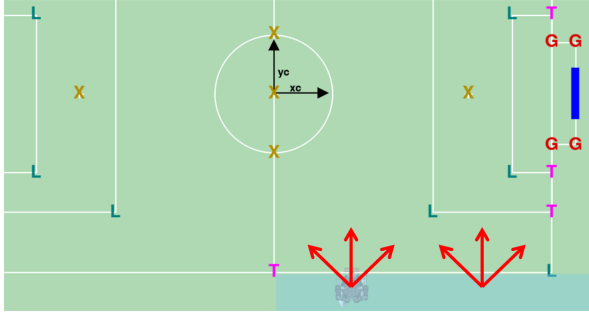


Fig. 4: The multi-hypothesis representation of the starting pose. The blue shaded area indicates the potential robot starting region, while the red arrows illustrate the six hypothesized poses.

According to the rules of RoboCup, the robot should start at the edge of our half side and face the field. Therefore, we use multi-hypothesis localization at the beginning of the match to find the pose. The initial hypothesis are shown in Fig. 4. We use the frame which receives more than 5 landmarks and set a threshold of 0.5 meter to the maximum matching error. We calculate the initial pose using all the hypothesis and the pose with smallest matching error will then be chosen as the initial pose. The others are abandoned. As we will show in the experiment part, the ILM method has a high tolerance on the initial position and orientation. Therefore, we do not need too much hypothesis.

C. Outlier Dropping

Since the pose estimation will be influenced by wrong matching, we need to drop the outlier. Fig. 5 shows our outlier dropping process. It uses the average matching error to check if it needs outlier dropping. If the average matching error is larger than 0.5 m, we check if there are enough landmarks in the frame. If there are more than 5 landmarks, we use RANSAC [33] method to find the outlier and recalculate the pose using inliers.

D. Filtering

In the competition, rules allowed for only a single IMU and a camera. We use filtering to fuse IMU data with localized estimates. The velocity of the robot is estimated using invariant extended Kalman filter (InEKF) [34] on

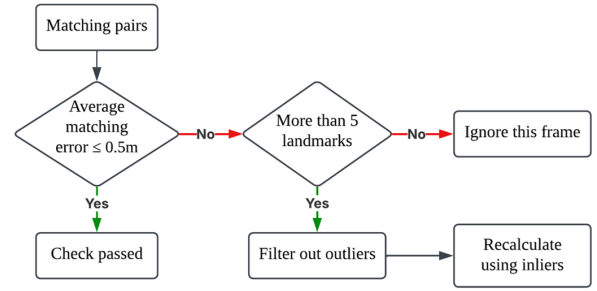


Fig. 5: The outlier dropping process

ARTEMIS. Two commonly used filter are Extended Kalman Filter (EKF) [35] and Particle Filter (PF) [36], [37].

Define the state vector X of the robot in 2D space and control input U as:

$$\mathbf{X}_k := [t_{x_k} \quad t_{y_k} \quad \theta_k]^T, \quad \mathbf{U}_k := [v_{fk} \quad v_{sk} \quad \omega_k]^T$$

where t_x and t_y represent the position of the robot, and θ represents its orientation. v_f is the forward velocity of the robot, v_s is the side velocity and ω is the angular velocity.

For discrete-time implementation, assuming a time step Δt , the state update equations become:

$$\mathbf{X}_{k+1} = \mathbf{X}_k + \begin{bmatrix} \cos(\theta_k) & -\sin(\theta_k) & 0 \\ \sin(\theta_k) & \cos(\theta_k) & 0 \\ 0 & 0 & 1 \end{bmatrix} \mathbf{U}_k \Delta t + \mathbf{W}_k$$

where \mathbf{W}_k represents the process noise. The measurement model is $\mathbf{Z}_k = \mathbf{X}_k + \mathbf{V}_k$, where \mathbf{V}_k is measurement noise, since ILM gives the \mathbf{X}_k directly. Since the measurement model is linear and the dynamic model is weakly nonlinear, both EKF [35] and PF [36], [37] work. We implemented particle filter in the RoboCup 2024 competition.

IV. EXPERIMENT RESULT

A. ILM vs ICP

We compare the ILM with the ICP in simulation and find that ILM method is more robust towards the error in the initial guess and easier to get a correct matching.

Fig. 6 shows the matching error under different initial guesses and different maximum allowable iterations for ILM. Fig. 7 shows the matching error using ICP. The true pose is $(t_x = 1, t_y = 1, \theta = 0)$. The initial guess t_{x_0}, t_{y_0} is equally sampled on the soccer field with $\theta_0 = 0$. The heatmaps show the matching error where dark purple means correct matching and bright yellow means incorrect matching.

Fig. 6 demonstrates that after a small number of iterations (5 times), the region for correct matching dramatically expands and has a high probability for correct matching. Comparing iteration 1 and iteration 8, we see that without iterative matching, the data association is correct only when the initial guess is close to the ground truth $(t_x = 1, t_y = 1, \theta = 0)$. After iterating 8 times, the correct region covers most of the whole field (86.67% of the field), which shows a large robustness for a wrong initial guess. The correct matching rate for random initial orientation for $(t_x = 1, t_y = 1, \theta = 0)$ is 52.78%, which is also quite large.

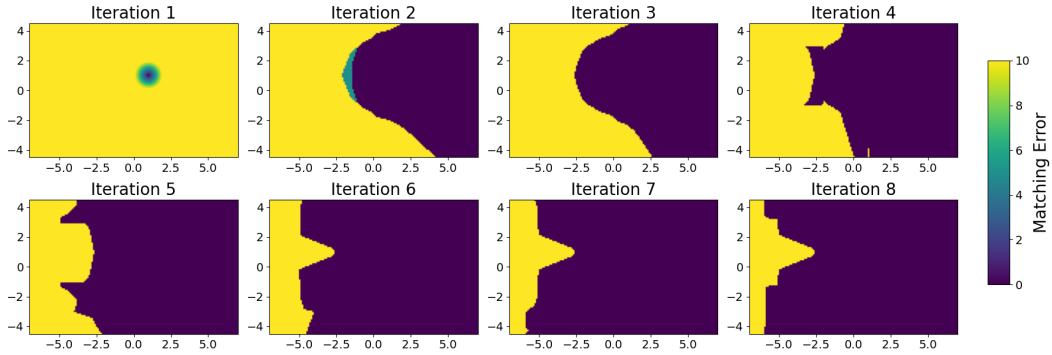


Fig. 6: Matching error of ILM using different initial guesses with different number of maximum allowable iterations. Dark purple means correct matching and bright yellow means incorrect matching

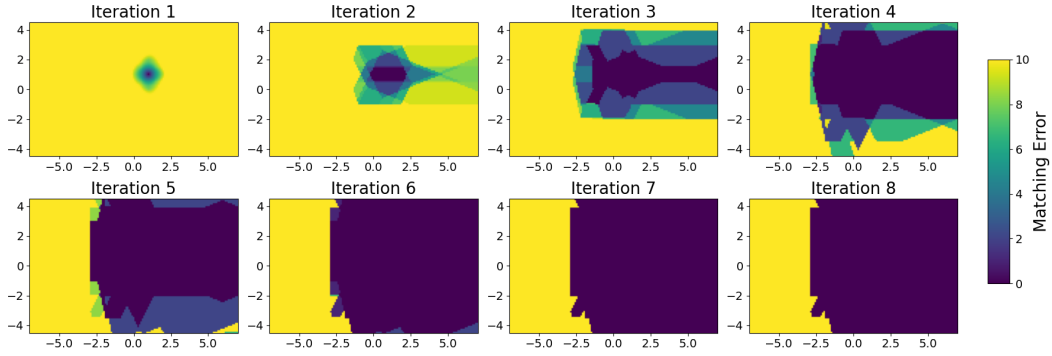


Fig. 7: Matching error of ICP using different initial guesses with different number of maximum allowable iterations. Dark purple means correct matching and bright yellow means incorrect matching

Comparing Fig. 6 and Fig. 7, the first 4 iterations show that ILM method finds the correct matching faster than ICP and the last 4 iterations show that the robustness for wrong initial guess using ILM is also larger than using ICP.

We do this analysis not only for the case ($t_x = 1, t_y = 1, \theta = 0$) but also across the entire soccer field, comparing the ILM and ICP methods, where the true position and orientation are equally sampled. The correct matching rates with random initial positions and orientations are shown in Fig. 8. In both subfigures, the blue surface represents ILM, and the red surface represents ICP. In all cases, the blue surface is above the red surface, indicating that ILM demonstrates higher tolerance to errors in both initial position and orientation.

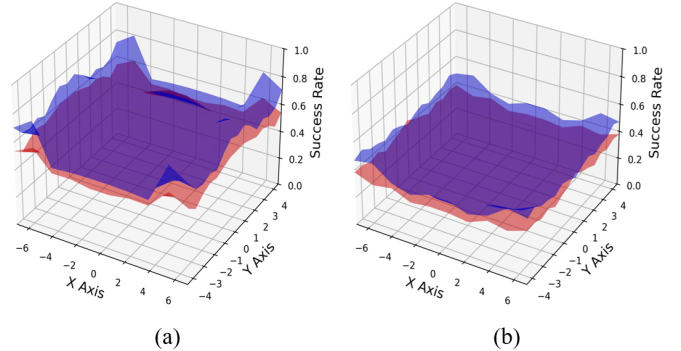


Fig. 8: Correct matching rate with random initial guess. (a) Initial position guess; (b) Initial orientation guess. Blue surface for ILM and red surface for ICP.

B. Simulation

We simulate a rectangular trajectory where the vertices are the corners of goal region. Uniformly sampled noise of ± 0.5 m is added to landmark observations. Uniformly sampled noise of ± 0.02 m is added to the position and ± 0.02 rad for orientation every 10 ms.

Fig. 9 depicts a trajectory with our method in blue and a trajectory purely with IMU data alone in black. The position and orientation error is shown in Fig. 10. We can see that our localization method works well under large sensor noise.

C. Field Test

In Fig. 11, ARTEMIS autonomously followed the desired trajectories using our path planning and following algorithm [1]. Three different types of trajectories were tested to verify the accuracy and robustness of our proposed localization method, as shown in Fig. 12. The trajectories appear unsmooth due to trajectory following errors and the periodic oscillations of the robot body in the bipedal locomotion. The robot completed five laps of each trajectory at a maximum speed of 1.0 m/s, with only the first lap shown for clarity. The ground truth pose was provided by the Vicon motion capture system in the lab. Due to the limited coverage area

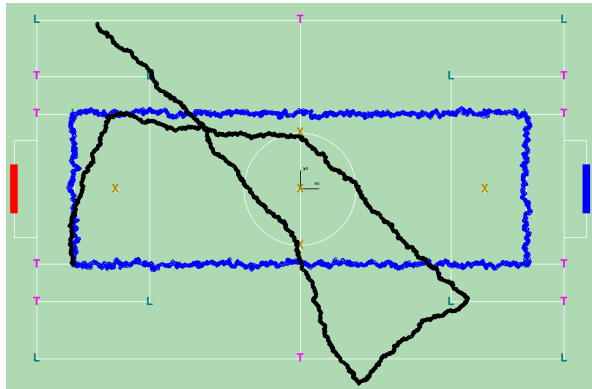


Fig. 9: Simulated trajectory using ILM (blue line) and only IMU (black line) for state estimation of a trajectory touching all 4 corners of the goal box.

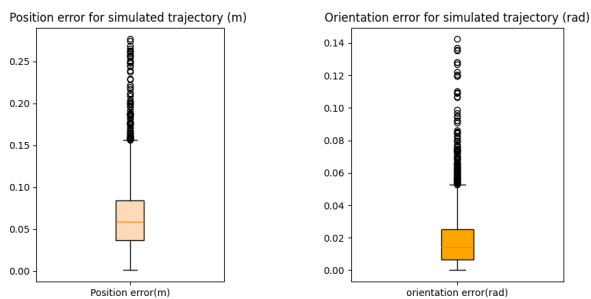


Fig. 10: Position and orientation errors for simulation trajectory.

of the mocap system, the three trajectories do not cover the entire soccer field. Localization results are shown in blue, while the ground truth position is shown in red. Some parts of the red line are disconnected due to mocap losing track of the markers.

Table I presents the Root Mean Square Error (RMSE), along with the minimum and maximum errors in position and orientation across the three trajectories. For comparative analysis, we implemented Augmented Monte Carlo Localization (aMCL) as introduced by Kim and Min [10], noted for its accuracy in real-time localization within the RoboCup environment. The particle count was configured to 200.

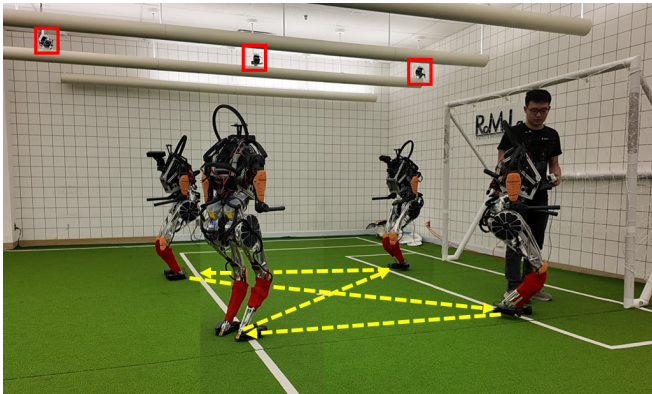


Fig. 11: A combined figure from different frames shows that ARTEMIS autonomously followed the X-shaped trajectory, indicated by yellow dashed lines. Motion capture cameras, enclosed in red boxes, provided the ground truth for the robot's pose.

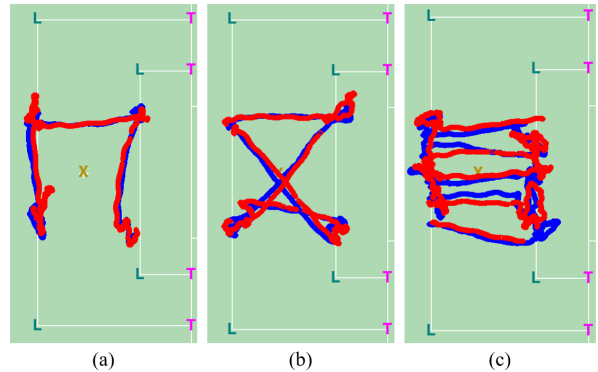


Fig. 12: Three tested trajectories in a real soccer field. (a): C-shape pattern; (b): X-shape pattern; (c): Zigzag pattern. The localization result is shown in blue, while the ground truth position from motion capture is in red.

TABLE I: Error statistics for different trajectories comparing ILM and aMCL.

(a) Position Error Statistics						
Trajectory	Position RMSE (meter)		Minimum Position Error (meter)		Maximum Position Error (meter)	
	ILM	aMCL	ILM	aMCL	ILM	aMCL
Trajectory 1	0.214	0.241	0.002	0.001	0.558	0.713
Trajectory 2	0.191	0.294	0.002	0.003	0.437	0.639
Trajectory 3	0.185	0.253	0.003	0.007	0.503	0.598

(b) Orientation Error Statistics						
Trajectory	Orientation RMSE (degree)		Minimum Orientation Error (degree)		Maximum Orientation Error (degree)	
	ILM	aMCL	ILM	aMCL	ILM	aMCL
Trajectory 1	3.189	3.282	0.0013	0.0007	8.316	12.127
Trajectory 2	4.092	4.197	0.0007	0.0013	12.974	14.673
Trajectory 3	3.231	3.012	0.0003	0.0004	12.218	16.050

Our localization method demonstrates accuracy comparable to that of aMCL, with slight improvements observed in certain instances. However, aMCL's average computation time is 0.0114 seconds (approximately 87.7 Hz), rendering it approximately ten times slower than our approach. Additionally, in scenarios where MCL particles exhibit significant divergence across the field, transitioning to the flipped pose is feasible due to the symmetric nature of the soccer field.

V. CONCLUSION

In this paper, we presented a fast, accurate, and robust vision-based 2D localization method capable of operating at approximately 1 kHz, achieving a positional RMSE of 0.2 m and an orientation RMSE of 3.5 degrees. This approach enables ARTEMIS to accurately estimate its real-time pose within a predefined soccer field. Field experiments demonstrated that our method outperformed adaptive Monte Carlo Localization (aMCL) with 200 particles in both accuracy and computational efficiency. Furthermore, comparisons between ILM and Iterative Closest Point (ICP) revealed that ILM exhibited greater robustness to errors in the initial pose estimate, leading to a higher rate of correct landmark matches.

REFERENCES

- [1] R. Hou, G. Fernandez, M. Zhu, and D. Hong, "Model predictive control with visibility graphs for humanoid path planning and tracking against adversarial opponents," in *2025 IEEE International Conference on Robotics and Automation*. (Accepted for publication).
- [2] G. Oriolo, A. Paolillo, L. Rosa, and M. Vendittelli, "Vision-based odometric localization for humanoids using a kinematic ekf," in *2012 12th IEEE-RAS International Conference on Humanoid Robots (Humanoids 2012)*. IEEE, 2012, pp. 153–158.
- [3] A. Kendall, M. Grimes, and R. Cipolla, "Posenet: A convolutional network for real-time 6-dof camera relocalization," in *Proceedings of the IEEE international conference on computer vision*, 2015, pp. 2938–2946.
- [4] G. I. Fernandez *et al.*, "Robocup 2024 adult-sized humanoid champions guide for hardware, vision, & strategy," in *Robot World Cup*. Springer, 2024.
- [5] T. Laue, T. J. De Haas, A. Burchardt, C. Graf, T. Röfer, A. Härtl, and A. Rieskamp, "Efficient and reliable sensor models for humanoid soccer robot self-localization," in *Proceedings of the Fourth Workshop on Humanoid Soccer Robots in conjunction with the*. Citeseer, 2009, pp. 22–29.
- [6] H. Schulz and S. Behnke, "Utilizing the structure of field lines for efficient soccer robot localization," *Advanced Robotics*, vol. 26, no. 14, pp. 1603–1621, 2012.
- [7] I. Nagi, W. Adiprawita, and K. Mutijarsa, "Vision-based monte carlo localization for robocup humanoid kid-size league," in *2014 13th International Conference on Control Automation Robotics & Vision (ICARCV)*. IEEE, 2014, pp. 1433–1438.
- [8] A. Muzio, L. Aguiar, M. R. Máximo, and S. C. Pinto, "Monte carlo localization with field lines observations for simulated humanoid robotic soccer," in *2016 XIII Latin American Robotics Symposium and IV Brazilian Robotics Symposium (LARS/SBR)*. IEEE, 2016, pp. 334–339.
- [9] G. Ficht, D. Pavlichenko, P. Allgeuer, H. Farazi, D. Rodriguez, A. Brandenburger, J. Kürsch, M. Schreiber, and S. Behnke, "Grown-up nimbros winning robocup 2017 humanoid adults size soccer competitions," in *RoboCup 2017: Robot World Cup XXI 11*. Springer, 2018, pp. 448–460.
- [10] J. Y. Kim, M. S. Ahn, and J. Han, "Enhancing adults size humanoid localization accuracy: A vision-based amcl leveraging object detection model and hungarian algorithm," in *2023 IEEE-RAS 22nd International Conference on Humanoid Robots (Humanoids)*. IEEE, 2023, pp. 1–8.
- [11] M. R. Dwijayanto, S. Kurniawan, and B. Sugandi, "Real-time object recognition for football field landmark detection based on deep neural networks," in *2019 2nd International Conference on Applied Engineering (ICAEE)*. IEEE, 2019, pp. 1–5.
- [12] S. Thrun, W. Burgard, and D. Fox, *Probabilistic Robotics*. MIT Press, 2005.
- [13] W. Hong, C. Zhou, and Y. Tian, "Robust monte carlo localization for humanoid soccer robot," in *2009 IEEE/ASME International Conference on Advanced Intelligent Mechatronics*. IEEE, 2009, pp. 934–939.
- [14] A. Hornung, K. M. Wurm, and M. Bennewitz, "Humanoid robot localization in complex indoor environments," in *2010 IEEE/RSJ International Conference on Intelligent Robots and Systems*. IEEE, 2010, pp. 1690–1695.
- [15] A. C. Almeida, A. H. Costa, and R. A. Bianchi, "Vision-based monte-carlo localization for humanoid soccer robots," in *2017 Latin American robotics symposium (LARS) and 2017 Brazilian symposium on robotics (SBR)*. IEEE, 2017, pp. 1–6.
- [16] P. J. Besl and N. D. McKay, "Method for registration of 3-d shapes," in *Sensor fusion IV: control paradigms and data structures*, vol. 1611. Spie, 1992, pp. 586–606.
- [17] Y. Chen and G. Medioni, "Object modelling by registration of multiple range images," *Image and vision computing*, vol. 10, no. 3, pp. 145–155, 1992.
- [18] A. Segal, D. Haehnel, and S. Thrun, "Generalized-icp," in *Robotics: science and systems*, vol. 2, no. 4. Seattle, WA, 2009, p. 435.
- [19] Y. Wang and J. M. Solomon, "Deep closest point: Learning representations for point cloud registration," in *Proceedings of the IEEE/CVF international conference on computer vision*, 2019, pp. 3523–3532.
- [20] Y. Aoki, H. Goforth, R. A. Srivatsan, and S. Lucey, "Pointnetlk: Robust & efficient point cloud registration using pointnet," in *Proceedings of the IEEE/CVF conference on computer vision and pattern recognition*, 2019, pp. 7163–7172.
- [21] J. Redmon, S. Divvala, R. Girshick, and A. Farhadi, "You only look once: Unified, real-time object detection," in *Proceedings of the IEEE conference on computer vision and pattern recognition*, 2016, pp. 779–788.
- [22] J. Terven, D.-M. Córdoba-Esparza, and J.-A. Romero-González, "A comprehensive review of yolo architectures in computer vision: From yolov1 to yolov8 and yolo-nas," *Machine learning and knowledge extraction*, vol. 5, no. 4, pp. 1680–1716, 2023.
- [23] H. W. Kuhn, "The hungarian method for the assignment problem," *Naval research logistics quarterly*, vol. 2, no. 1-2, pp. 83–97, 1955.
- [24] J. Munkres, "Algorithms for the assignment and transportation problems," *Journal of the society for industrial and applied mathematics*, vol. 5, no. 1, pp. 32–38, 1957.
- [25] R. Jonker and T. Volgenant, "A shortest augmenting path algorithm for dense and sparse linear assignment problems," in *DGOR/NSOR: Papers of the 16th Annual Meeting of DGOR in Cooperation with NSOR/Vorträge der 16. Jahrestagung der DGOR zusammen mit der NSOR*. Springer, 1988, pp. 622–622.
- [26] M. Selmaier, S. Hamzehi, and K.-J. Meier, "Evaluation of algorithm performance for simulated square and non-square logistic assignment problems," *ECMS*, pp. 16–26, 2021.
- [27] D. B. Malkoff, "Evaluation of the jonker-volgenant-castanon (jvc) assignment algorithm for track association," in *Signal Processing, Sensor Fusion, and Target Recognition VI*, vol. 3068. SPIE, 1997, pp. 228–239.
- [28] D. F. Crouse, "On implementing 2d rectangular assignment algorithms," *IEEE Transactions on Aerospace and Electronic Systems*, vol. 52, no. 4, pp. 1679–1696, 2016.
- [29] M. Levedahl, "Performance comparison of 2d assignment algorithms for assigning truth objects to measured tracks," in *Signal and Data Processing of Small Targets 2000*, vol. 4048. SPIE, 2000, pp. 380–389.
- [30] W. Kabsch, "A solution for the best rotation to relate two sets of vectors," *Acta Crystallographica Section A: Crystal Physics, Diffraction, Theoretical and General Crystallography*, vol. 32, no. 5, pp. 922–923, 1976.
- [31] K. S. Arun, T. S. Huang, and S. D. Blostein, "Least-squares fitting of two 3-d point sets," *IEEE Transactions on pattern analysis and machine intelligence*, no. 5, pp. 698–700, 1987.
- [32] C. R. Maurer, G. B. Aboutanos, B. M. Dawant, R. J. Maciunas, and J. M. Fitzpatrick, "Registration of 3-d images using weighted geometrical features," *IEEE transactions on medical imaging*, vol. 15, no. 6, pp. 836–849, 1996.
- [33] M. FISCHLER AND, "Random sample consensus: a paradigm for model fitting with applications to image analysis and automated cartography," *Commun. ACM*, vol. 24, no. 6, pp. 381–395, 1981.
- [34] M. S. Ahn, "Development and real-time optimization-based control of a full-sized humanoid for dynamic walking and running," in *PhD Thesis*. University of California, Los Angeles, 2023.
- [35] J. Kim, Y. Kim, and S. Kim, "An accurate localization for mobile robot using extended kalman filter and sensor fusion," in *2008 IEEE International Joint Conference on Neural Networks (IEEE World Congress on Computational Intelligence)*. IEEE, 2008, pp. 2928–2933.
- [36] C. Chen and D. Schonfeld, "A particle filtering framework for joint video tracking and pose estimation," *IEEE Transactions on Image Processing*, vol. 19, no. 6, pp. 1625–1634, 2010.
- [37] O. Tariq and D. Han, "2d particle filter accelerator for mobile robot indoor localization and pose estimation," *IEEE Access*, 2024.